The Effect of Microstructure on Fracture Toughness and Fatigue Crack Growth Behavior in γ-Titanium Aluminide Based Intermetallics

J.P. CAMPBELL, K.T. VENKATESWARA RAO, and R.O. RITCHIE

Ambient-temperature fracture toughness and fatigue crack propagation behavior are investigated in a wide range of ($\gamma + \alpha_2$) TiAl microstructures, including single-phase γ, duplex, coarse lamellar (1 to 2 mm colony size (D) and 2.0 μm lamellar spacing (λ)), fine lamellar ($D \sim 150$ μm, $\lambda = 1.3$ to 2.0 μm), and a powder metallurgy (P/M) lamellar microstructure ($D = 65$ μm, $\lambda = 0.2$ μm). The influences of colony size, lamellar spacing, and volume fraction of equiaxed γ grains are analyzed in terms of their effects on resistance to the growth of *large* (>5 mm) cracks. Specifically, coarse lamellar microstructures are found to exhibit the best cyclic and monotonic crack-growth properties, while duplex and single-phase γ microstructures exhibit the worst, trends which are rationalized in terms of the salient micromechanisms affecting growth. These mechanisms primarily involve crack-tip shielding processes and include crack closure and uncracked ligament bridging. However, since the potency of these mechanisms is severely restricted for cracks with limited wake, in the presence of *small* (<300 μm) cracks, the distinction in the fatigue crack growth resistance of the lamellar and duplex microstructures becomes far less significant.

I. INTRODUCTION

THE γ-TiAl–based intermetallic alloys have received considerable attention in recent years as candidate materials for high-temperature aerospace applications,[1,2] with the most recent efforts being directed toward the replacement of Ni-based superalloys in the lower-pressure, lower-temperature regions at the rear of the turbine.[1,3,4] Titanium aluminides based on the γ phase (TiAl) exhibit densities which are, respectively, ~15 and 50 pct lower than those of Ti- and Ni-based alloys, while maintaining satisfactory oxidation resistance, creep resistance, and elevated-temperature strength for the targeted applications. Specific composition/microstructure combinations are believed to be capable of satisfactory performance at operating temperatures up to ~ 760 °C.[1,3] These alloys, thus, offer the potential of improved engine efficiency and performance *via* higher operating temperatures and improved thrust-to-weight ratios. Application of these materials is hindered, however, by low ambient-temperature ductility and questionable fracture toughness and fatigue crack growth resistance.

Previous investigations have revealed that fracture toughness and fatigue crack growth resistance of coarse lamellar microstructures (~1- to 2-mm-sized colonies of alternating γ and α_2 lamellae*) are superior to those of duplex microstructures (primarily equiaxed γ grains with equiaxed α_2 or fine lamellar colonies).[3,6–10] However, the superior crack-growth resistance of the coarse lamellar microstructures may be seen as questionable, due to the scale of the microstructure in relation to the sample sizes employed.[6,11] With typical specimen thickness dimensions on the order of 5 mm in several studies of the coarser-lamellar microstructures (colony size greater than 0.75 mm),[6,7,12,13] a mere 2 to 6 lamellar colonies exist along the crack front; statistical sampling of the microstructure is, thus, inadequate, and true polycrystalline constraint is not developed at the crack tip. In such cases, the measured fracture and fatigue properties of lamellar microstructures may be dependent on specimen geometry and size. In addition to these questions concerning the superior crack-growth resistance of the lamellar microstructure, the strength and ductility in lamellar materials are generally lower than those of duplex structures.

In view of this, recent research efforts have focused on refining the lamellar microstructures, both in terms of reducing lamellae[14–17] and colony dimensions.[15,16,18–22] However, the effects of such microstructural variations on the fracture properties are poorly understood. Accordingly, the objective of the present work is to examine the ambient-temperature fracture toughness and fatigue crack–growth performance (long crack and small crack) of a series of dual phase ($\gamma + \alpha_2$) TiAl alloys with a wide range of microstructures, including duplex, fully lamellar with coarse colony size, fully lamellar with refined colony size, nearly lamellar with refined colony size, and a powder metallurgy (P/M) fully lamellar material with refined colony size and refined lamellar thickness. The results of this study suggest that the improved (long crack) toughness and fatigue crack growth resistance of specific microstructures largely results from crack-tip shielding mechanisms (*e.g.*, uncracked ligament bridging and crack closure) which act to reduce the

*Although many interfaces are γ/α_2, γ/γ twin boundaries also occur.[5]

J.P. CAMPBELL, Graduate Student Researcher, is with the Department of Materials Sciences and Mineral Engineering, University of California, Berkeley, CA. R.O. RITCHIE, Professor, is with the Materials Science Division, Lawrence Berkeley National Laboratory, and Department of Materials Science and Mineral Engineering, University of California, Berkeley, CA 94720-1760. K.T. VENKATESWARA RAO, formerly Research Engineer with the Department of Materials Science and Mineral Engineering, University of California, Berkeley, CA, is Manager, R & D, Vascular Intervention Group, Guidant Corporation, Santa Clara, CA 95052.

Manuscript submitted April 21, 1998

local driving force for crack growth. However, the benefit of such toughening mechanisms is not realized in the presence of microstructurally small cracks.

II. EXPERIMENTAL PROCEDURES

A. *Materials*

Four γ-TiAl–based intermetallic alloys were examined in the present study. Relevant microstructural features and mechanical properties are given, respectively, in Tables I and Table II. The first material, a Ti-47.7Al-2.0Nb-0.8Mn (at pct) alloy containing ~1 vol pct TiB_2 particles was fabricated by the XD* process (a proprietary method for incorporating *in situ* ceramic reinforcements[23]). This alloy was permanent mold–cast into 40-mm-diameter rods and then hot isostatically pressed (''HIPed'') at 1260 °C and 172 MPa for 4 hours. The resulting nearly lamellar microstructure (Figure 1(a)), hereafter referred to as *XD nearly lamellar*, contained refined lamellar colonies (~120 μm in diameter) with lamellar spacing (λ) (center-to-center distance of the α_2 phase) of 2.0 μm, ~30 pct equiaxed γ grains and the TiB_2 phase randomly distributed as needle-like particles (20 to 50 μm in length, 2 to 5 μm in diameter) among the γ grains and lamellar colonies.*

*XD is a trademark of Lockheed Martin, Bethesda, MD.

*For all microstructures, grain and colony dimensions were measured using optical microscopy, whereas lamellar spacings were determined using backscattered electron images from a scanning electron microscope.

The second alloy, Ti-47Al-2Nb-2Cr-0.2B (at. pct), was first two-step forged at 1150 °C (70 pct reduction per step), with a recrystallization heat treatment (1260 °C for 4 hours in argon, argon gas furnace cooled) in between. A lamellar microstructure was then produced by heat treating the alloy in flowing argon gas at 1370 °C for 1 hour, air cooling, and holding for 6 hours at 900 °C prior to argon gas furnace cooling. The resulting microstructure (Figure 1(b)), referred to as *MD fully lamellar*, consisted of refined lamellar colonies (145-μm diameter) with a lamellar spacing of 1.3 μm and less than 4 pct of fine equiaxed γ grains (5 to 20 μm) between lamellar colonies. A corresponding duplex microstructure (Figure 1(c)), referred to as *MD duplex*, was obtained by furnace cooling following heating at 1320 °C for 3 hours in argon. The structure consisted of nearly equiaxed grains of the γ phase (~17 μm in diameter) with ~10 vol pct α_2 (Ti_3Al) present as thin layers (~1 to 3-μm thick) at grain boundaries or as larger ''blocky'' regions (~3 to 23 μm in diameter) at triple-point grain intersections; a small amount of fine lamellar colonies was also present. In both microstructures boron additions to the alloy resulted in ~0.5 vol pct of needle-like TiB_2 particles (~2 to 10 μm in length, ~1 μm in diameter).

The third alloy studied was prepared by P/M techniques using a starting powder of composition Ti-47Al-2Nb-2Cr (at pct), with subsequent elevated-temperature extrusion and heat treatment to create a fully lamellar microstructure with an order of magnitude smaller lamellar spacing. This microstructure (Figure 1(d)), referred to as *P/M lamellar*, consisted of refined lamellar colonies (~65 μm in diameter) with very fine lamellae (average α_2 spacing of 0.22 μm) and less than 5 pct very fine equiaxed γ grains (~1 μm in diameter) at the colony boundaries. The processing and microstructural features of this alloy are presented in detail elsewhere.[14]

The behavior of the aforementioned microstructures is compared to results previously reported in a fourth alloy, Ti-47.3Al-2.3Nb-1.5Cr-0.4V (at pct).[6]* This material was produced by skull melting and casting techniques,[8] and was subsequently HIPed at 1150 °C and 275 MPa for 3 hours and isothermally forged at 1150 °C to about 90 pct reduction. A coarse lamellar microstructure (Figure 1(e)), referred to as *G7 coarse lamellar*, was produced by annealing for 2 hours at 1370 °C, cooling at 30 °C/min to 900 °C, and then aging for 5 hours at 900 °C before air cooling. Colony sizes in this microstructure were on the order of 1 to 2 mm, with similar lamellar spacing (λ = 1.3 μm) to the XD and MD materials (Table 1). A corresponding duplex microstructure (Figure 1(f)), referred to as *G7 duplex*, was produced by annealing for 2 hours at 1300 °C, cooling at 100 °C/min to 900 °C, aging for 5 hours at 900 °C, and air cooling.

*As noted previously, due to the coarseness of the lamellar microstructure in this alloy with respect to typical test sample dimensions, results for this structure are likely to be geometery dependent.

B. *Experimental Techniques*

Fatigue crack growth studies on long ($a > 5$ mm) through-thickness cracks in all microstructures were performed in room-temperature air (22 °C, 45 pct relative humidity) using 4- to 5-mm-thick compact-tension specimens. Tests were conducted at a sinusoidal frequency of 25 Hz using servohydraulic testing machines operated under automated stress-intensity (K) control, in general accordance with ASTM standard E647. A constant load ratio (R), equal to K_{min}/K_{max}, of 0.1 (tension-tension) was maintained, where K_{min} and K_{max} are the minimum and maximum stress intensities of the loading cycle, respectively. Fatigue thresholds (ΔK_{TH}) were operationally defined as the applied stress–intensity range corresponding to growth rates below $\sim 10^{-10}$ m/cycle and were approached using variable ΔK/constant R load-shedding schemes. Crack lengths were continuously monitored using back-face strain compliance methods and/or electrical-potential measurements on NiCr foil gages bonded to the side face of the specimen.

Elastic compliance data were also utilized to measure the extent of crack-tip shielding from crack closure and crack bridging. Crack closure was evaluated in terms of the closure stress intensity (K_{cl}), which was approximately defined at the load corresponding to the first deviation from linearity on the unloading compliance curve.[25,26] Crack bridging was assessed using a method[27] of comparing the experimentally measured unloading compliance (at loads above those associated with closure) to the theoretical value for a traction-free crack.[28,29,30] Optical measurement of the crack length was required for evaluation of the theoretical compliance. With this technique, a bridging stress intensity (K_{br}), representing the reduction in K_{max} due to the bridging tractions developed in the crack wake, can be estimated.

The corresponding crack-growth behavior of small ($c <$ 300 μm) surface cracks was investigated using unnotched rectangular beams (width (W) of 10 mm, thickness of 6 mm, and span of 50 mm), loaded in four-point bending.

Table I. Microstructure of γ-TiAl–Based Alloys

Microstructure/Composition (At. Pct)	Lamellar Colony Size, D	Lamellar Spacing, λ*	Equiaxed γ Phase	γ Grain Size
XD nearly lamellar/ Ti-47.7Al-2.0Nb-0.8Mn + 1 vol pct TiB_2	120 μm	2.0 μm	~30 pct	~23 μm
MD fully lamellar/ Ti-47Al-2Nb-2Cr-0.2B	145 μm	1.3 μm	~4 pct	5 to 20 μm
MD duplex/ Ti-47Al-2Nb-2Cr-0.2B	—	—	90 pct	17 μm
P/M lamellar/ Ti-47Al-2Nb-2Cr	65 μm	0.2 μm	<5 pct	~1 μm
G7 coarse lamellar/ Ti-47.3Al-2.3Nb-1.5Cr-0.4V**	1 to 2 mm	1.3 μm	<5 pct	10 to 40 μm
G7 duplex/ Ti-47.3Al-2.3Nb-1.5Cr-0.4V**	—	—	90 to 95 pct	15 to 40 μm

*Center-to-center spacing of the α_2 phase.
**From Ref. [6].

Table II. Mechanical Properties of γ-TiAl–Based Alloys

Microstructure/Composition (At. Pct)	Yield Strength (MPa)	Fracture Strength (MPa)	Elongation (Pct)	Fracture Toughness* (MPa $\sqrt{m}$)
XD nearly lamellar**/ Ti-47.7Al-2.0Nb-0.8Mn + 1 vol pct TiB_2	546	588	0.7	12 to 16
MD fully lamellar/ Ti-47Al-2Nb-2Cr-0.2B	426	541	0.8	18 to 32
MD duplex/ Ti-47Al-2Nb-2Cr-0.2B	384	489	0.9	—
P/M lamellar/ Ti-47Al-2Nb-2Cr	975	1010	1.0	18 to 22
G7 coarse lamellar/ Ti-47.3Al-2.3Nb-1.5Cr-0.4V	450	525	1.0	18 to 39
G7 duplex/ Ti-47.3Al-2.3Nb-1.5Cr-0.4V	450	590	4.0	11

*A range in values indicates R-curve behavior; the first value corresponds to the crack-initiation toughness, K_i; the second to the steady-state toughness or maximum measured crack-growth resistance, K_{ss}.
**Tensile data are taken from a material of similar composition and microstructure.[24]

Cracking was initiated under cyclic tensile loading from electrodischarge machining pit damage; the rapid, localized heating and cooling associated with the electrical discharge produced small cracks in the vicinity of the pit. Samples were then cyclically loaded to grow the cracks away from the heat-affected zone (HAZ) prior to data acquisition (the HAZ was easily identified optically using an aqueous 2 pct HF/5 pct H_3PO_4 etchant on a polished surface). In some instances, sample surfaces were ground and polished following pitting to completely eliminate the HAZ, leaving only small cracks on the surface. Using this procedure, initial surface flaws with half-surface lengths (c) less than ~125 μm were readily achieved.

Bend samples were cycled at $R = 0.1$ at between 5 and 25 Hz (sine wave), with crack lengths monitored by periodic surface replication using cellulose acetate tape. Replicas were Au or Pt coated to improve resolution, and corresponding crack lengths were measured optically. Average growth rates were computed from the amount of crack extension between two discrete measurements. Stress intensities were determined using linear-elastic solutions for surface cracks in bending,[31] assuming a semicircular crack profile (crack-depth to half-surface-crack length ratio (a/c) of 1). This assumption was verified by heat tinting specific samples at 600 °C for 4 hours prior to fracture and subsequent optical observation of the crack shape; measurements revealed an average a/c ratio of 1.04, which corresponds to a semicircular crack.

Fracture toughness behavior was characterized in terms of $K_R(\Delta a)$ resistance R-curves, *i.e.*, monotonic crack-growth resistance (K_R) as a function of crack extension (Δa) using fatigue-precracked compact-tension specimens (of identical size to those used for fatigue studies). Tests were conducted by monotonically loading samples under displacement control until crack extension was initiated. Following crack extension, the sample was unloaded by ~10 pct of the peak load at extension, the crack length was recorded using an optical telescope, and the sample was reloaded until further

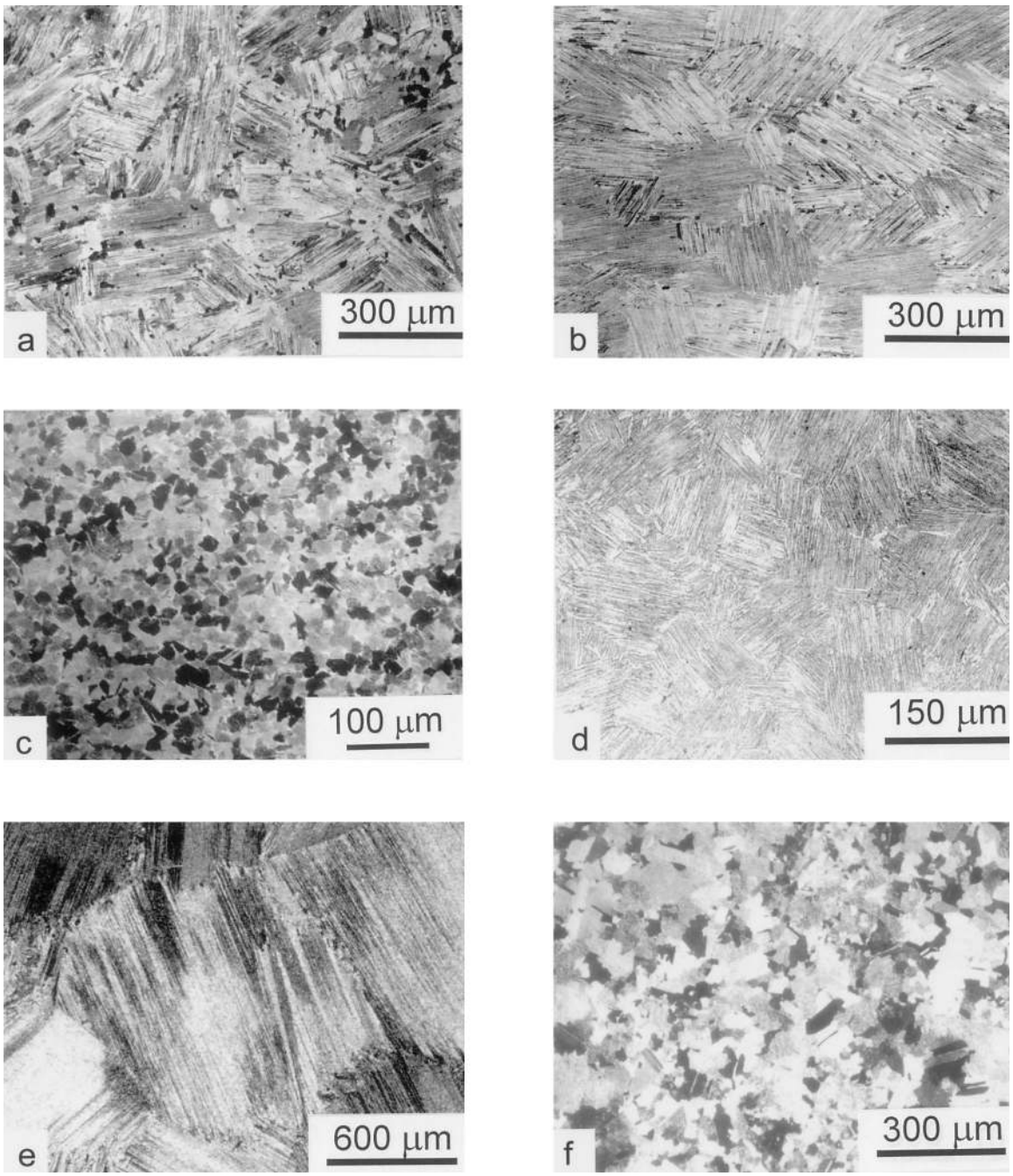

Fig. 1—Optical micrographs of (*a*) Ti-47.7Al-2.0Nb-0.8Mn + 1 vol pct TiB_2 (XD nearly lamellar), (*b*) Ti-47Al-2Nb-2Cr-0.2B (MD fully lamellar), (*c*) Ti-47Al-2Nb-2Cr-0.2B (MD duplex), (*d*) Ti-47Al-2Cr-2Nb (P/M lamellar), (*e*) Ti-47.3Al-2.3Nb-1.5Cr-0.4V (G7 coarse lamellar), and (*f*) Ti-47.3Al-2.3Nb-1.5Cr-0.4V (G7 duplex) microstructures.

crack extension occurred. This sequence was repeated until the final sample fracture or termination of the test. Applied-load and crack-length measurements were used to calculate the stress intensities at extension, in general accordance with ASTM standard E399.

The nature of the crack path and its wake were investigated using scanning electron microscopy (SEM) of crack profiles, imaged both at the surface and, after sectioning and polishing, at the specimen midthickness (plane-strain region). The SEM images were recorded in backscatter electron imaging mode at accelerating voltages from 10 to 20 kV and a working distance of 10 mm.

III. RESULTS AND DISCUSSION

A. *Fracture Toughness Behavior*

The fracture toughness behavior of the XD nearly lamellar, MD fully lamellar, G7 coarse lamellar, P/M lamellar, and G7 duplex microstructures is compared in terms of $K_R(\Delta a)$ R-curves in Figure 2 with results[32] for a single-phase γ microstructure (Ti-55 at. pct Al, with traces of Nb, Ta, C, and O).

The coarsest microstructure, the G7 coarse lamellar, clearly displays the highest toughness and steepest R-curve behavior, with a crack-initiation toughness (K_i) of ~18

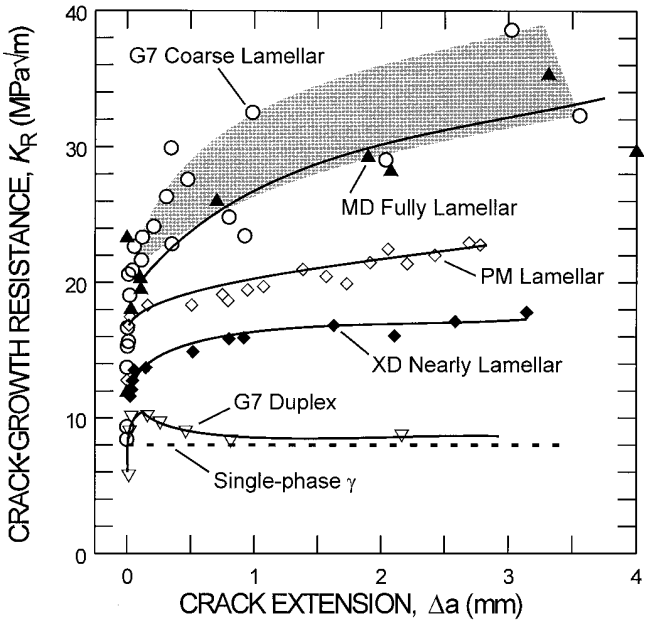

Fig. 2—Monotonic fracture toughness behavior in the form of $K_R(\Delta a)$ resistance curves for the MD fully lamellar, P/M lamellar, and XD nearly lamellar microstructures. Also shown for comparison is behavior in the G7 coarse lamellar, G7 duplex, and single-phase γ microstructures.

MPa$\sqrt{m}$ and a maximum crack-growth toughness (K_{ss}) of ~32 to 39 MPa$\sqrt{m}$ after ~3 mm of crack extension. The development of such R-curve toughening in lamellar γ-TiAl–based alloys can be attributed primarily to the formation of uncracked (''shear'') ligaments of lamellar colonies in the crack wake.[33,34] These ligament bridges, which result from the inability of both inter- and intralamellar microcracks to link with the main crack tip, contribute to toughening by providing bridging tractions across the crack faces, thereby shielding the crack tip from the far-field loading, and by plastic dissipation within the ligaments. Previous studies have indicated that the initiation toughness in lamellar microstructures is improved relative to that in duplex and single-phase γ structures by crack deflection and branching, microcracking ahead of the crack tip, crack-tip blunting in the α_2 phase, and slip and twinning in the γ phase.[5,9,35–37]

The single-phase γ and G7 duplex microstructures exhibit the lowest toughnesses, with negligible R-curve behavior and respective K_i values of 8 and 11 MPa$\sqrt{m}$. Indeed, the finer γ-TiAl–based duplex structures are known to exhibit far lower toughnesses than the lamellar materials. The lack of R-curve behavior is attributed to minimal formation of uncracked ligament bridges in the duplex microstructure.[6,8,38]

Refinement of the lamellar microstructure, specifically the colony size, lowers the toughness. However, despite an order of magnitude decrease in colony size (D) between the G7 coarse lamellar (D = 1 to 2 mm) and the MD fully lamellar (D = 145 μm) structures, the fracture resistance of the finer MD fully lamellar microstructure is only slightly lower than that the of the G7 coarser lamellar material, with K_i ~18 MPa$\sqrt{m}$ and K_{ss} ~ 32 MPa$\sqrt{m}$ after 4 mm of crack extension in the MD material. Conversely, the XD nearly lamellar microstructure has essentially the same small colony size as the MD fully lamellar material, yet exhibits ~50 pct lower R-curve toughness, *i.e.*, its toughness is only marginally better than the duplex structure, with initiation and maximum growth toughnesses of K_i ~ 12 and K_{ss} ~ 16 MPa$\sqrt{m}$, respectively.

Refinement of the lamellar spacing has mixed effects. The P/M lamellar material has roughly half the colony size and a factor of 5 times smaller lamellar spacing than the MD and XD fine lamellar structures, yet exhibits a toughness intermediate to these two microstructures, with K_i ~ 17 MPa$\sqrt{m}$ and K_{ss} ~ 22 MPa$\sqrt{m}$ after 3 mm of crack extension. These toughness values are in reasonable agreement with the value of 22.4 MPa$\sqrt{m}$ reported by Liu *et al.* for the same material.[14] It is interesting to note, however, that the toughness values reported for the P/M lamellar TiAl are lower than those reported by Liu *et al.*[39] for cast and hot-extruded γ-TiAl–based alloys of similar composition, where the reported toughnesses ranged from ~ 30 to 60 MPa$\sqrt{m}$ for lamellar microstructures with refined colony and lamellae dimensions. Presumably, the apparent disparity in the reported toughness values for these refined lamellar structures arises in part from the technique employed to evaluate fracture toughness in the cast + hot-extruded materials. In this case, the toughness was evaluated from a chevron-notched bend beam (no fatigue precrack) using a correlation between toughness and the work of fracture.[40] As Liu *et al.* point out, this technique provides only an estimation of the true fracture toughness. Furthermore, Liu *et al.* also reported that, for the particular sample geometry employed, plane-strain conditions were likely violated for toughness values exceeding ~30 MPa$\sqrt{m}$. Both the lack of a fatigue precrack and the violation of plane-strain conditions likely result in an overestimation of the true plain-strain fracture toughness for the cast + hot-extruded γ-based TiAl materials.

1. *The relative influence of colony size and lamellar spacing on toughness*

It is expected that microstructural parameters such as the lamellar spacing and lamellar colony size will influence toughness; Chan and Kim noted that the effect of these microstructural dimensions on crack-growth toughness results from their influence on the size and area fraction of uncracked ligaments which form in the crack wake.[34,41] Consistent with intuition, the magnitude of shielding attributed to uncracked ligament bridging was found to increase with increasing ligament size and area fraction.

Chan and co-workers have noted that, for sufficiently small lamellar spacing, *e.g.*, $\lambda < \sim 1$ μm, K_i and K_{ss} are independent of λ,[42] while, for $\lambda > \sim 1$ μm, both K_i and K_{ss} vary inversely with λ in a manner similar to the Hall–Petch relation.[41,42] The results of the present study are consistent with these observations. Specifically, a constant crack-initiation toughness, K_i ~ 18 MPa$\sqrt{m}$, is observed for all three fully lamellar microstructures, where the α_2 center-to-center spacing ranges from 0.2 to 1.3 μm. However, the K_{ss} value was not found to be constant; instead, it ranged from 22 to 39 MPa$\sqrt{m}$. As discussed below, this observation is presumably related to the fact that K_{ss} is influenced by the lamellar colony size when the plastic zone size (r_y) is larger than the colony dimensions ($D/r_y < 1$),[41] as is the case for the MD fully lamellar, XD nearly lamellar, and P/M lamellar microstructures.

Chan and Kim[41] have suggested a relatively complex

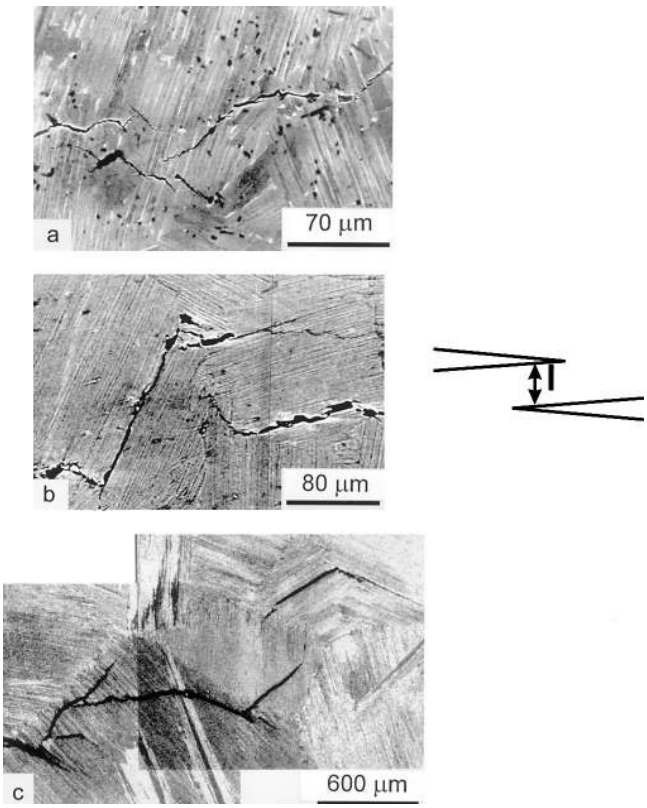

Fig. 3—Crack wake profiles showing uncracked ligament bridges in the (*a*) XD nearly lamellar, (*b*) MD fully lamellar, and (*c*) G7 coarse lamellar microstructures. These samples were subjected to resistance curve testing. The profiles (a) and (b) were recorded in the SEM operating in backscatter electron imaging mode to provide phase contrast (α_2 phase appears light in contrast, the γ phase is gray, and TiB_2 particles appear black). Profile (c) is an optical micrograph.

dependence of toughness on colony size. Specifically, the steady-state toughness in various lamellar γ-TiAl–based intermetallics was found to increase with increasing colony size until a critical value of D was attained; this critical colony size was found to correspond approximately to the crack-tip plastic zone size (r_y) at K_{ss}. For further increases in colony size, such that $D/r_y > 1$, the crack-tip plastic zone tends to be embedded within a single lamellar colony. In such cases, the steady-state toughness is governed primarily by the lamellar spacing and is also influenced by the lamellae orientation within a colony. In the present study, only the G7 coarse lamellar microstructure meets the criterion for the steady-state toughness to be governed primarily by λ, with r_y ($=K^2/[2\pi\sigma_y^2]$) = 1258 μm and D/r_y = 1.2 at K_{ss}. In the XD nearly lamellar (r_y = 137 μm), MD fully lamellar (r_y = 789 μm), and P/M lamellar microstructures (r_y = 81 μm), the respective values of D/r_y at K_{ss} are 0.9, 0.2, and 0.8; presumably, both D and λ have significant influence on the steady-state toughness in these materials. Based on this discussion, it is likely that the lower steady-state toughness of the P/M lamellar microstructure, relative to that exhibited by the other fully lamellar microstructures, results from the small colony size (65 μm) and comparable magnitudes of D and r_y (*i.e.*, development of the bridging zone and, hence, toughness, is strongly influenced by both D and λ). Although the P/M lamellar microstructure has a relatively lower toughness than the G7 coarse lamellar and MD fully lamellar microstructures, it should be noted that this alloy has a yield strength at least twice that of the other fully lamellar materials. Its strength/toughness combination is clearly of interest.

2. *On the influence of characteristic bridging-zone parameters*

Regardless of which microstructural parameter governs the uncracked ligament size and area fraction, it is important to realize that it is ultimately the characteristics of the bridging zone which will determine the bridge shielding contribution to toughness. Although toughness in the MD fully lamellar and G7 coarse lamellar materials is predicted to be governed by different microstructural parameters (primarily λ in the G7 and both λ and D in the MD), it is interesting to note that the two microstructures, possessing equal lamellar spacing, have a nearly equivalent toughness despite an order of magnitude difference in colony diameter. Comparatively, the XD nearly lamellar microstructure, with both D and λ roughly equivalent to that in the MD fully lamellar material, exhibits significantly lower toughness. As will be discussed later, these results suggest that relatively small uncracked ligaments can result in monotonic crack-growth resistance comparable to that observed in high-toughness, coarse lamellar microstructures with much larger uncracked ligaments, provided that the number of small bridges (as reflected by the area fraction of bridging ligaments (f) and bridging zone length (L)) is high.

The bridging zones of the XD nearly lamellar, MD fully lamellar, and G7 coarse lamellar structures were characterized using metallographic sections of crack-wake profiles (two profiles per condition), taken perpendicular to the crack plane in the plane-strain region at center thickness (Figure 3). The zones were evaluated in terms of the following parameters:

(1) the average ligament size (l, the dimension of the ligament in a direction perpendicular to the crack faces and the crack-growth direction (Figure 3, inset));
(2) the area fraction of uncracked ligaments in the bridging zone (f, measured as a line fraction of ligaments on a crack-wake profile); and
(3) the bridging-zone length (L, measured as the furthest distance of an intact ligament from the crack tip).

Average values are listed in Table III.

The parameters in Table III indicate that the MD fully lamellar and XD nearly lamellar materials exhibit equivalent area fractions of bridging ligaments, whereas the bridging-zone length and average ligament size are, respectively, ~60 and 130 pct larger in the MD fully lamellar material. Comparatively, the area fraction of bridging ligaments in the G7 coarse lamellar microstructure is approximately half of that for the XD and MD materials, but the reported bridging ligament height is larger. The bridging-zone length for the G7 coarse lamellar material is comparable to that in the XD nearly lamellar and less than that for the MD fully lamellar structure.

More succinctly stated, the bridging zone in the G7 coarse lamellar microstructure exhibits relatively fewer and larger uncracked ligaments, while the bridging ligaments in the MD fully lamellar and XD nearly lamellar microstructure are larger in number but smaller in size (note relative ligament sizes in Figure 3). Using the bridging-zone param-

Table III. Characterizing Parameters for Uncracked Ligament Bridging in Lamellar TiAl Microstructures

Microstructure	Average Ligament Size, l (μm)	Ligament Area Fraction, f	Bridging Zone Length, L (mm)	Bridging Contribution to Toughness, K_{br} (MPa $\sqrt{m}$)*
MD fully lamellar	72	0.20	4.9	14
XD nearly lamellar	31	0.21	3.1	4
G7 coarse lamellar**	201	0.135	3.0	14 to 21

*The toughness contribution of the bridging ligaments is taken as $K_{br} = K_{ss} - K_i$, where K_{ss} is the maximum measured crack-growth resistance and K_i is the initiation toughness (Fig. 2).

**l and f were not measured in the G7 coarse lamellar microstructure; the reported values are for a material of similar microstructure and composition (sample 366 in Ref. 34).

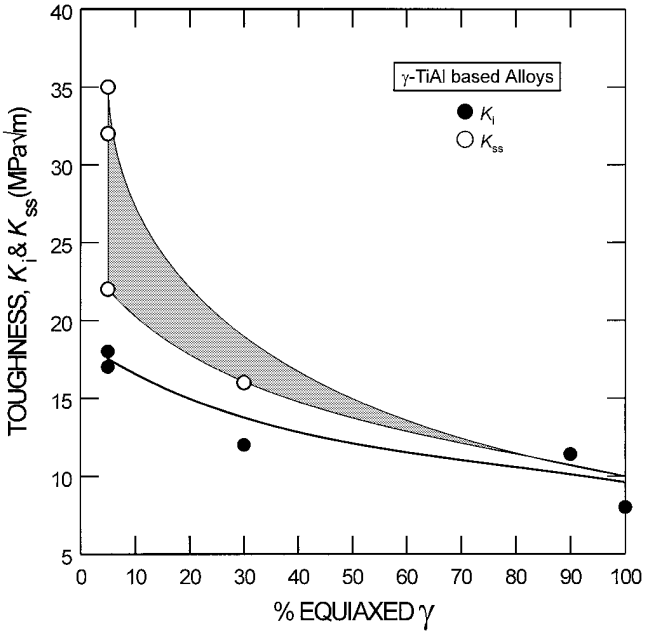

Fig. 4—Relationships between toughness (K_i and K_{ss}) and volume fraction of equiaxed γ phase for several γ-TiAl–based microstructures (MD fully lamellar, XD nearly lamellar, P/M lamellar, G7 coarse lamellar, G7 duplex, and single-phase γ). It is apparent that the equiaxed γ phase degrades toughness.

eters indicated in Table III, these characteristics of the uncracked ligament bridging zones can be described in terms of the volume of the material in the bridging ligaments per unit thickness (V), assuming a through-thickness crack. Specifically,

$$V = lfL \qquad [1]$$

Although it has been shown that fracture toughness in lamellar TiAl alloys correlates well with the product lf,[34] given the importance of plastic deformation and redundant fracture within the ligaments to the toughness,[5,33,36] it seems logical that the entire volume of material in the crack-wake ligaments (*i.e.*, the product of $V = lfL$) is the more physically meaningful parameter. However, provided that bridging-zone lengths do not vary significantly, either parameter, lf or V, will correlate well with K_{br}.

Taking a V value of 1 for the G7 coarse lamellar structure, the relative values for the MD fully lamellar and XD nearly lamellar microstructures are 0.87 and 0.25, respectively. In the case of the two fully lamellar structures (G7 and MD), the distinctly different bridging zones have comparable values of V and nearly equivalent toughness, as represented by the $K_R(\Delta a)$ R-curves in Figure 2. The disparity in toughness between the MD fully lamellar and XD nearly lamellar microstructures is attributed to there being smaller and fewer bridging ligaments and, hence, a significantly lower value of V in the XD material (note the relative values of l and L in Table III), as well as to the presence of ~30 pct equiaxed γ phase in the XD nearly lamellar material.

3. *Role of equiaxed γ*

The presence of equiaxed γ grains has a significant influence on toughness and, particularly, on bridge formation. The XD nearly lamellar structure, where the low toughness is associated with reduced uncracked ligament bridge formation, has a volume fraction of ~30 pct of equiaxed γ grains, compared to less than 5 pct in the other lamellar structures studied. This effect is even more pronounced in the duplex and single-phase γ microstructures, which have >90 pct equiaxed γ grains; these structures develop negligible uncracked ligament formation and, therefore, exhibit little or no R-curve behavior.[6,32] In general, the presence of the equiaxed γ phase is detrimental to both the initiation and R-curve toughness; this is clear in Figure 4, where values of K_i and K_{ss} for all the microstructures studied display an inverse relationship to the volume fraction of equiaxed γ phase in each structure. This same observation regarding the degradation of crack-growth resistance has been previously reported for fracture toughness (K_{IC}).[43] and R-curve crack-initiation toughness.[42] Chan attributes the increase K_i with increasing volume fraction of lamellar structure to the beneficial effect of enhanced crack-tip blunting in these regions of the microstructure. As will be discussed in Section III–B–1, a similar deleterious effect of the equiaxed γ phase on fatigue crack growth thresholds is observed.

B. *Fatigue Crack Propagation Behavior*

1. *Role of microstructure*

a. *Growth-rate behavior*

The variations in long crack ($a > 5$ mm), fatigue crack growth rates (da/dN) as a function of the applied stress–intensity range, for the XD nearly lamellar, MD fully lamellar, MD duplex, G7 coarse lamellar, G7 duplex, and P/M lamellar microstructures, are compared in Figure 5 to previous data[32] for an ~2- to 10-μm-grain-sized, single-phase γ alloy (Ti-55 at. pct Al, with traces of Nb, Ta, C, and O). In general, the lamellar microstructures show superior fatigue crack growth resistance compared to the equiaxed γ-grain alloys (duplex and single-phase γ), consistent with previous observations.[3,6,7] As with the R-curve results (Figure 2), the G7 coarse lamellar displays the best (long crack) properties; in fact, the rank ordering of all the microstructures, in terms

of fatigue crack growth resistance, parallels exactly their relative toughness under monotonic loading.

For all alloys and microstructures, crack growth rates are a strong function of ΔK, particularly in the duplex microstructures, where the entire *da/dN vs* ΔK curve lies within a ΔK range of ≤ 1 MPa$\sqrt{\text{m}}$. Comparatively, the lamellar microstructures show the greater damage tolerance, with higher crack-growth thresholds and improved *da/dN vs* ΔK slopes in the midgrowth-rate regime ($\sim 10^{-9}$ to 10^{-6} m/cycle). Measured fatigue crack–growth thresholds and Paris-law ($da/dN \propto \Delta K^m$) exponents for the midgrowth-rate regime are shown in Table IV.

b. *Microstructural factors*

The various lamellar microstructures investigated, differing in colony size, lamellar spacing, and volume fraction of equiaxed γ grains, display a range of cyclic crack-growth resistance nearly as large as that observed between the lamellar and duplex structures. While the G7 coarse lamellar microstructure exhibits the best fatigue crack growth resistance, the MD fully lamellar material possesses only slightly lower crack-growth resistance despite an order of magnitude reduction in colony size. The difference is largest at near-threshold levels, where $\Delta K_{TH} \sim 8.6$ MPa$\sqrt{\text{m}}$ for the MD fully lamellar structure, compared to $\Delta K_{TH} \sim 10$ MPa$\sqrt{\text{m}}$ for the coarser G7 structure. The XD nearly lamellar microstructure, on the other hand, with a colony size ($\sim$120 μm) roughly equivalent to that of the MD fully lamellar material ($\sim$145 μm), displays significantly lower crack-growth resistance. In fact, the XD nearly lamellar structure shows only marginally better near-threshold properties ($\Delta K_{TH} \sim 7.1$ MPa$\sqrt{\text{m}}$) than the duplex alloys ($\Delta K_{TH} \sim 6.5$ and 5.9 MPa$\sqrt{\text{m}}$ for the G7 and MD duplex structures, respectively); its relative fatigue resistance, however, is improved at growth rates above $\sim 10^{-8}$ m/cycle.

The most prominent microstructural difference between the XD nearly lamellar and MD fully lamellar materials is the high volume fraction ($\sim$30 pct) of equiaxed γ grains present in the XD structure. The other microstructures with high volume fractions of equiaxed γ grains, *i.e.*, the single-phase γ, G7 duplex, and MD duplex alloys, all show the lowest fatigue crack growth resistance (Figure 5). These observations suggest a deleterious correlation between fatigue crack growth resistance and equiaxed γ grains, which is illustrated in Figure 6, where ΔK_{TH} is plotted as a function of the volume fraction of equiaxed γ phase; the trend parallels the degradation in toughness due to the presence of the equiaxed γ grain (Figure 4). It is believed that the equiaxed γ grains degrade crack growth resistance by inhibiting the activity of extrinsic shielding mechanisms, specifically, crack closure (where the γ grains allow for a less-tortuous crack path) and uncracked ligament bridging[33,35] (where the γ grains do not participate in the ligament formation).

Refinements in the lamellar dimensions, as in the higher-strength P/M lamellar microstructure, where the α_2 center-to-center spacing is $\sim$0.22 μm (with a colony size of $\sim$65 μm),[14] did not induce further improvements in fatigue performance (Figure 5); the crack-growth resistance was found to be intermediate to that of the XD nearly lamellar (α_2 spacing of $\sim$2.0 μm) and MD fully lamellar (α_2 spacing of $\sim$1.3 μm) microstructures.

2. *Crack-tip shielding mechanisms*

The disparity in fatigue crack growth resistance between the duplex and lamellar microstructures and between the various lamellar structures can be principally related to differences in the degree of crack-tip shielding provided by crack closure and uncracked ligament bridges.* These two shielding mechanisms are quite different in character; crack closure is a process that induces crack wedging and is created during fatigue crack growth, whereas uncracked ligament bridging can be generated under monotonic loading and is actually degraded under cyclic loads. To examine these phenomena quantitatively, we will focus on the XD and MD alloys.

*It is important to note that these are *extrinsic* shielding mechanisms which act in the crack wake to impede crack growth by reducing the local driving force actually experienced at the crack tip. In the absence of a crack wake, *i.e.*, for crack initiation or small-crack growth behavior, their effect becomes minimal. They are distinct from *intrinsic* fatigue mechanisms, which are associated with microstructural damage mechanisms ahead of the crack tip.[44,45]

a. *Crack closure*

Measured crack-closure data, for the XD nearly lamellar, MD fully lamellar, and MD duplex structures, are presented in Figure 7(a) in the form of closure stress–intensity values (K_{cl}) as a function of ΔK. It is clear that closure plays a role at all ΔK levels in all of these microstructures, as K_{cl} values are always greater than those of $K_{\min}$. Of the three alloys examined, closure levels were highest in the MD fully lamellar microstructure, where K_{cl} values range from $\sim$ 4 to 7 MPa$\sqrt{\text{m}}$ with increasing ΔK. Although there is considerable scatter in the measured values for this structure, a trend of increasing K_{cl} with increasing ΔK is observed. The rise in K_{cl} is believed to be associated with the formation of uncracked ligament bridges at higher ΔK values. Although the interpretation of crack closure in the presence of bridging is uncertain, the present results definitely suggest an enhanced closure effect in this microstructure.

b. *Uncracked ligament bridging*

As described previously, uncracked ligament bridging has been well documented[5,6,35,36,41] as an important toughening mechanism under monotonic loading in γ-TiAl–based lamellar microstructures. However, many such bridging mechanisms, which induce significant *R*-curve toughening under monotonic loads, *e.g.*, ductile-phase reinforcements, can become ineffective during cyclic loading.[32,46,47] This results from a cyclic degradation of the bridges or from an inability of the bridges to form at the lower stress intensities typical of fatigue. Indeed, this argument has been previously applied to uncracked ligaments formed during fatigue loading in the MD fully lamellar material[48] and in a similar lamellar γ-TiAl–based material.[49] Specifically, Chan and Shih reported that uncracked ligaments formed during fatigue crack growth are subject to cyclic degradation, and that this degradation can be attributed to higher strain levels in the ligaments than ahead of the crack tip. However, the extent to which the shielding contribution of such ligaments is reduced has not been quantified. In the present study, direct microscopic examination of the crack wake confirms that uncracked ligament bridges do form in lamellar structures during cyclic loading (Figure 8); similar evidence of bridge formation during fa-

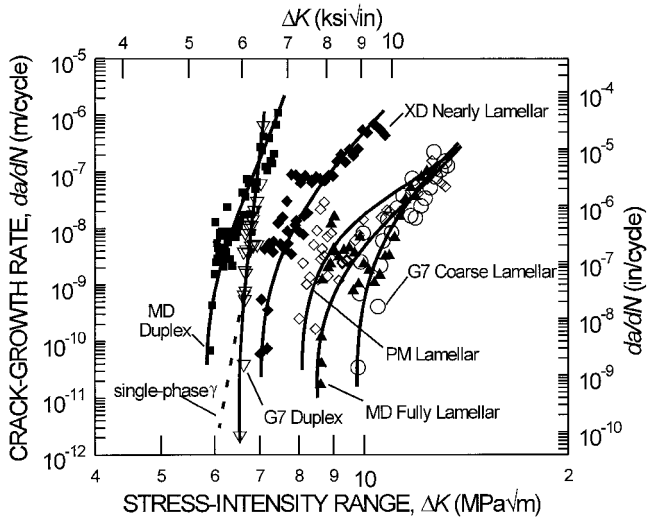

Fig. 5—Fatigue crack growth resistance in the MD fully lamellar, MD duplex, XD nearly lamellar, P/M lamellar, G7 coarse lamellar, G7 duplex, and single-phase γ microstructures. In general, the lamellar microstructures show superior fatigue crack growth resistance compared to the equiaxed γ structures (*i.e.*, duplex and single-phase γ). The various lamellar microstructures investigated display a range of cyclic crack growth resistance nearly as large as that observed between the lamellar and duplex structures.

Table IV. Fatigue Crack Growth Behavior in γ-Base TiAl Alloys

Microstructure/Composition (At. Pct)	Midgrowth Rate Regime* Paris Exponent, m	Fatigue Threshold, ΔK_{TH} (MPa $\sqrt{m}$)
XD nearly lamellar/ Ti-47.7Al-2.0Nb-0.8Mn + 1 vol pct TiB_2	15	7.1
MD fully lamellar/ Ti-47Al-2Nb-2Cr-0.2B	9	8.6
MD duplex/ Ti-47Al-2Nb-2Cr-0.2B	22	5.7
G7 coarse lamellar/ Ti-47.3Al-2.3Nb-1.5Cr-0.4V	15	10
G7 duplex/ Ti-47.3Al-2.3Nb-1.5Cr-0.4V	50	6.5
P/M lamellar/ Ti-47Al-2Nb-2Cr	8	8.2

*For 10^{-9} to 10^{-8} m/cycle $\leq da/dN \leq 10^{-6}$ m/cycle.

tigue crack growth in lamellar TiAl microstructures was reported in Reference 50. While the shielding which results from these ligaments is substantially reduced from that seen under monotonic loading, it is not eliminated.

An example of such an uncracked ligament, imaged at sample midthickness in the MD fully lamellar structure, is shown in Figure 8(a), where cycling had been maintained at a constant ΔK of 11.3 MPa$\sqrt{m}$ ($R = 0.1$); here, the value of the maximum stress intensity ($K_{max} = 12.6$ MPa$\sqrt{m}$) is well below the initiation toughness for crack growth under monotonic loads ($K_i \sim 18$ MPa$\sqrt{m}$). Corresponding analyses in the XD nearly lamellar structure, however, indicated that uncracked ligament bridges were only observed to form in fatigue at high ΔK levels, where K_{max} was greater than K_i; an example is shown in Figure 8(b), where K_{max} (equal to 13 MPa$\sqrt{m}$) is just above the R-curve initiation toughness of $K_i \sim 12$ MPa$\sqrt{m}$. Thus, whereas uncracked ligament bridge formation during fatigue crack growth was prevalent in the MD fully lamellar structure at K levels well below K_i, it was only present in the XD nearly lamellar microstructure at high K_{max} levels exceeding K_i (where monotonic crack-growth mechanisms frequently become operative). Indeed, no bridge formation was observed at lower ΔK levels in the XD microstructure, although cracks did show a small tendency to deflect, branch, and form secondary cracks.

In order to quantify the magnitude of shielding from uncracked ligament bridging in the XD and MD lamellar microstructures, bridging stress intensities (K_{br}), representing the reduction in K_{max} due to the bridging tractions, were estimated by comparing the measured and theoretical unloading compliance, as discussed in Section II–B. Results are presented in Figure 7(a), where K_{max}, K_{min}, and ($K_{max} - K_{br}$) are plotted as a function of ΔK (for $R = 0.1$); the magnitude of shielding provided by uncracked ligaments is given by the difference between the K_{max} and ($K_{max} - K_{br}$) lines (Figure 7(b)). These results confirm that the influence of bridging is insignificant in the XD nearly lamellar alloy; specifically, measured K_{br} values are merely $\sim$ 2 to 4 pct of K_{max} (*e.g.*, $K_{br} = 0.2$ and 0.5 MPa$\sqrt{m}$ at $\Delta K = 7.8$ and 11.7 MPa$\sqrt{m}$, respectively). Although the extent of bridging is also low in the MD fully lamellar structure at near-threshold levels (*e.g.*, $K_{br} = 0.5$ MPa$\sqrt{m}$ at $\Delta K = 8.6$ MPa$\sqrt{m}$), it becomes increasingly significant with increasing ΔK, with $K_{br} = 2.1$ MPa$\sqrt{m}$ (14 pct of K_{max}) at $\Delta K = 12.6$ MPa$\sqrt{m}$. It should be emphasized here that this shielding contribution in fatigue is substantially lower than that occurring during monotonic fracture, where K_{br} (equal to $K_{ss} - K_i$) $\sim$ 14 MPa$\sqrt{m}$ (Figure 2, Table III). Note that no uncracked ligament bridging was detected in the duplex material.

Thus, quantitative measurements of the magnitude of crack closure and bridging in the XD nearly lamellar and MD fully lamellar alloys confirm that the effect of shielding is far more significant in the latter microstructure, consistent with its superior fatigue crack growth resistance. Moreover, the greater propensity in this microstructure for uncracked ligament bridge formation under cyclic loading is consistent with its superior R-curve behavior under monotonic loads (Figure 2).

c. *Crack deflection*

Initial, qualitative optical observations of fatigue-crack profiles at the compact-tension sample surface in the XD nearly lamellar and MD fully lamellar microstructures suggested a significant disparity between these materials in the degree of crack-tip shielding due to crack deflection; the crack profile of the MD fully lamellar microstructure appeared significantly more deflected. However, subsequent measurements on crack profiles of sectioned samples (in the plane-strain region) revealed little difference in the extent of crack deflection. Average crack deflection angles, (θ_{avg}) in the plane-strain region for the XD nearly lamellar

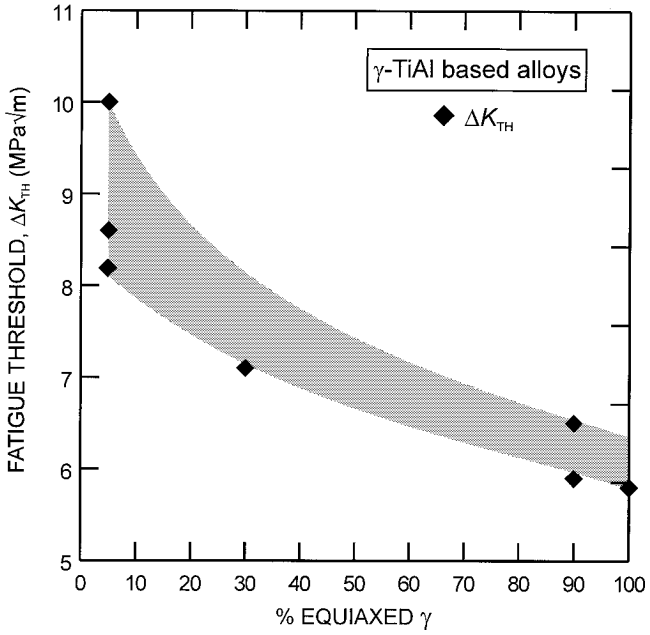

Fig. 6—The fatigue crack growth threshold, ΔK_{TH}, as a function of the volume fraction of equiaxed γ grains in several γ-TiAl–based microstructures (MD fully lamellar, MD duplex, XD nearly lamellar, P/M lamellar, G7 coarse lamellar, G7 duplex, and single-phase γ). A deleterious correlation between fatigue crack growth resistance and the equiaxed γ phase is observed.

and MD fully lamellar microstructures are, respectively, 29.6 and 28.6 deg at a ΔK of 7.8 and 9.4 MPa$\sqrt{\text{m}}$, respectively. The average deflection angle in the MD fully lamellar microstructure increases only slightly with increasing ΔK (θ_{avg} = 32.1 deg at a ΔK of 12.5 MPa$\sqrt{\text{m}}$). Furthermore, application of a model for crack deflection[51] revealed a negligible shielding effect (shielding <3.5 pct of K_{max}).

d. *Intrinsic vs extrinsic crack-growth resistance*

Based on these measured closure and bridging stress intensities (Figure 7(a)), the overall crack-tip shielding contribution can be quantified by defining an effective (near-tip) stress–intensity range (ΔK_{eff}),

$$\Delta K_{eff} = (K_{max} - K_{br}) - K_{cl} \quad [2]$$

(where $K_{cl} > K_{min}$), as illustrated in Figure 7(b). For the MD and XD lamellar microstructures, the shielding correction was applied to crack growth rates at applied ΔK values within 0.5 MPa$\sqrt{\text{m}}$ of the stress intensity ranges at which K_{br} was measured. This allowed for plotting a sufficient number of shielding-corrected data points; it was assumed that the true values of K_{br} would not vary significantly over this small range of ΔK. Plotting the measured fatigue crack growth rates as a function of the closure- and bridging-corrected ΔK_{eff} confirms that shielding by closure and bridging are the prime mechanisms responsible for the differences in the fatigue crack growth resistance of the various microstructures (Figure 9).

For example, in the MD alloy, growth rates in the fully lamellar and duplex microstructures, which are quite different when characterized in terms of the applied ΔK, are nearly scaled when characterized in terms of ΔK_{eff} (Figure 9(a)). Indeed, the difference in the fatigue thresholds is reduced from ~3 MPa$\sqrt{\text{m}}$, when characterized in terms of ΔK, to only ~1 MPa$\sqrt{\text{m}}$ in terms of ΔK_{eff} ($\Delta K_{TH,eff}$ = 4.3 and 5.5 MPa$\sqrt{\text{m}}$, respectively, for the duplex and lamellar structures). These results suggest that the difference in the *intrinsic* fatigue crack growth resistance of the lamellar and duplex microstructures is small.

The prominent role of shielding is also important in rationalizing the differences in crack-growth resistance exhibited by the various lamellar microstructures. For example, growth rates in the XD nearly lamellar and MD fully lamellar microstructures differ by roughly one to two orders of magnitude when compared at the same applied ΔK levels; however, when characterized in terms of the

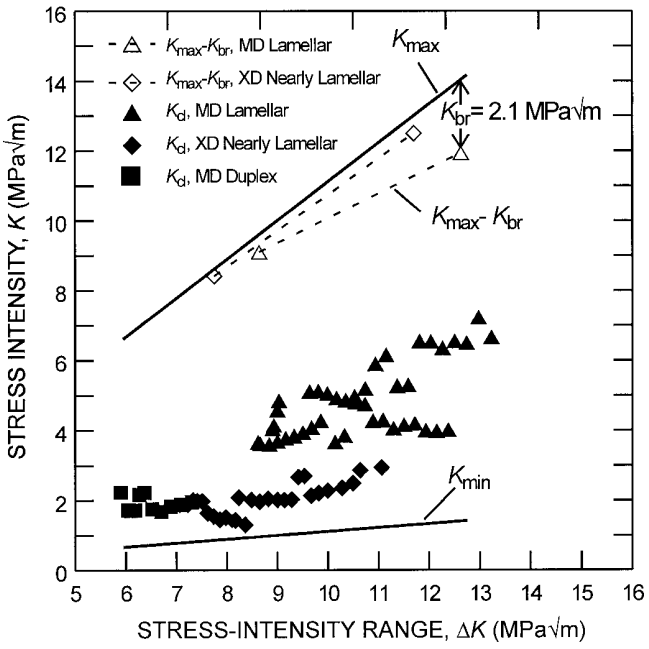

(*a*)

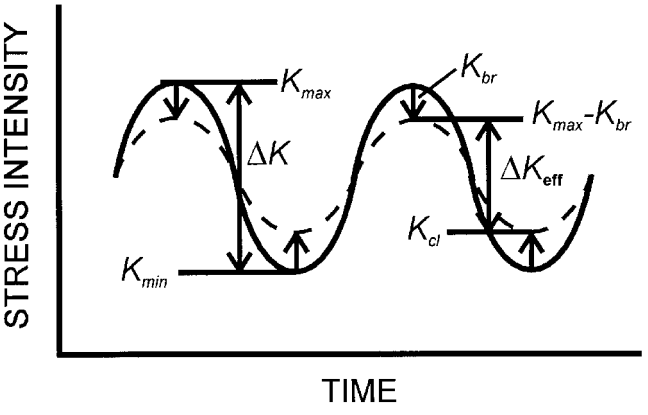

(*b*)

Fig. 7—(*a*) Experimentally measured crack-shielding stress intensities are plotted as a function of ΔK at R = 0.1. Crack closure stress intensities, K_{cl}, are shown for the MD fully lamellar, MD duplex, and XD nearly lamellar microstructures. The magnitude of shielding provided by uncracked ligament bridging, K_{br}, is given by the difference between the K_{max} and K_{max}-K_{br} lines. (*b*) This schematic plot of stress intensity as a function of time illustrates the capability of uncracked ligament bridging and crack closure to reduce the stress intensity range experienced at the crack tip to $\Delta K_{eff} = (K_{max} - K_{br}) - K_{cl}$.

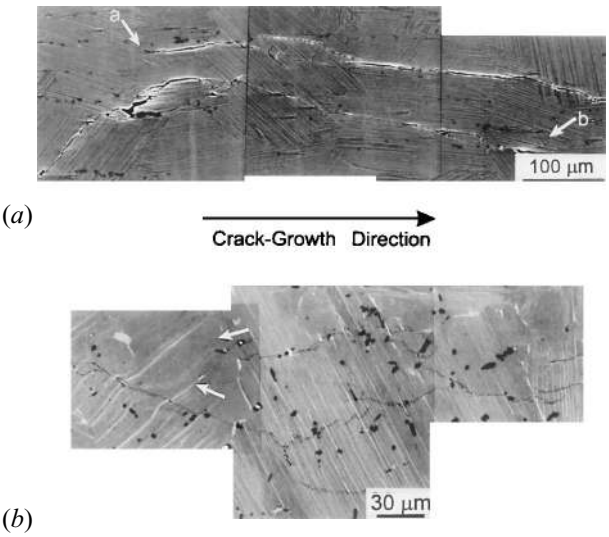

(*a*)

(*b*)

Fig. 8—Scanning electron micrographs of fatigue crack profiles (at sample midthickness) in the (*a*) MD fully lamellar and (*b*) XD nearly lamellar microstructures, which illustrate the presence of uncracked ligament bridges. The respective loading conditions for the crack profile regions in (a) and (b) are ΔK = 12.5 and 11.7 MPa$\sqrt{\text{m}}$ (R = 0.1 for both). In (a), the arrows a and b indicate the beginning of the crack at the top of the bridge and the end of the crack at the bottom of the bridge. The γ, α_2, and TiB_2 phases appear, respectively, light, gray, and black in contrast.

closure- and bridging-corrected ΔK_{eff}, these differences are virtually eliminated (Figure 9(b)).* In fact, their effective thresholds are identical ($\Delta K_{TH,\text{eff}} \sim$ 5.5 MPa$\sqrt{\text{m}}$). Again, these results strongly suggest that the *intrinsic* fatigue crack growth properties of these various γ-TiAl–based alloy microstructures are not that different.

*The increased scatter at higher growth rates for the shielding-corrected data in the MD fully lamellar microstructure in Figure 9 results principally from scatter in the measured K_{cl} values (Figure 7(a)).

e. *Comparison of bridging under monotonic and cyclic loading*

It is well known that many bridging mechanisms, for example, ductile-phase ligaments in intermetallic composites[32,46,47] or interlocking grains in monolithic ceramics (*e.g.*, Reference 52), are severely degraded under cyclic loading conditions. Accordingly, an experiment was performed to quantify the extent to which the current uncracked ligament bridging mechanisms are diminished in fatigue. Specifically, a steady-state bridging zone was developed by monotonically loading a compact-tension specimen of the MD fully lamellar microstructure along the R curve to a K_R of ~30 MPa$\sqrt{\text{m}}$. The sample was then cyclically loaded (25 Hz sine wave, R = 0.1) for over 3 × 10^5 cycles (3.5 hours) at ΔK = 10 MPa$\sqrt{\text{m}}$, and the extent of bridge degradation was monitored through changes in the back-face strain compliance and was quantified in terms of the associated changes in the value of K_{br}. No crack extension occurred during the cycling due to the shielding from the pre-existing bridging zone. Results are shown in Figure 10, where it can be seen that the bridging zone developed under monotonic loading exhibited a bridging stress intensity of 5.5 MPa$\sqrt{\text{m}}$ at the start of cyclic loading.* After 875 fatigue cycles, the bridging had decreased by 35 pct to $K_{br} \sim$ 3.6 MPa$\sqrt{\text{m}}$; subsequently, no further degradation was observed out to 3.15 × 10^5 loading cycles. Based on these observations, it is clear that uncracked ligament bridging will degrade under cyclic loading, although this bridging mechanism appears to be more resilient than

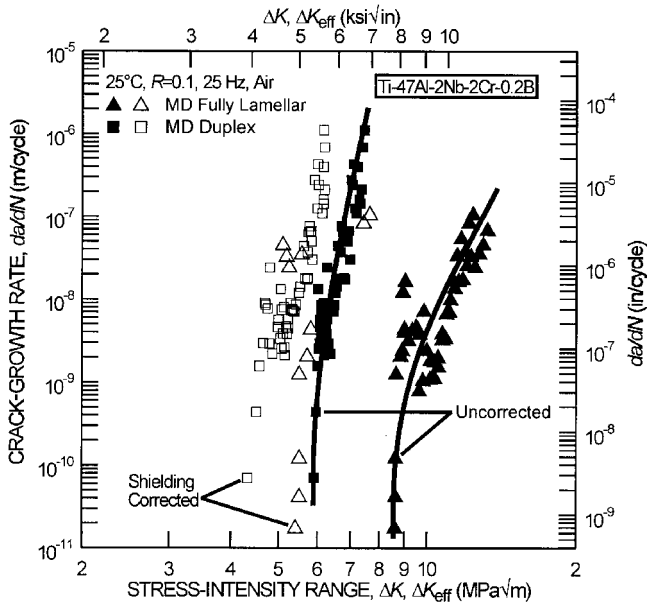

(*a*)

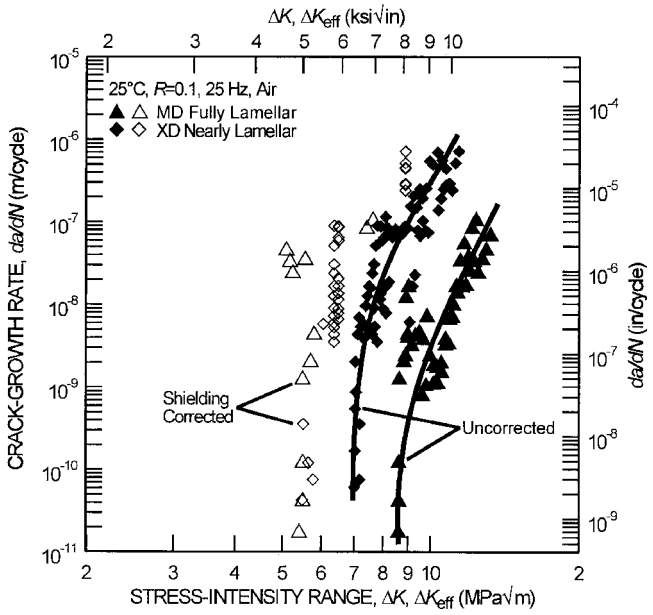

(*b*)

Fig. 9—Fatigue-crack growth rates, *da*/*dN*, for long cracks in (*a*) the MD fully lamellar and MD duplex microstructures and (*b*) the MD fully lamellar and XD nearly lamellar microstructures are plotted as a function of the applied stress intensity range, ΔK, and an effective, near-tip stress intensity range, ΔK_{eff}, from which the effect of extrinsic crack shielding mechanisms (closure and bridging) have been ''subtracted.''

*The shielding contribution of a given bridging zone scales linearly with the applied stress intensity; therefore, the value of K_{br} at the start of cyclic loading is less than that observed during the initial monotonic (R curve) loading (where K_{br} was as high as 12 MPa$\sqrt{\text{m}}$), simply due to the lower value of $K_{\max}$ at the applied cyclic loads.

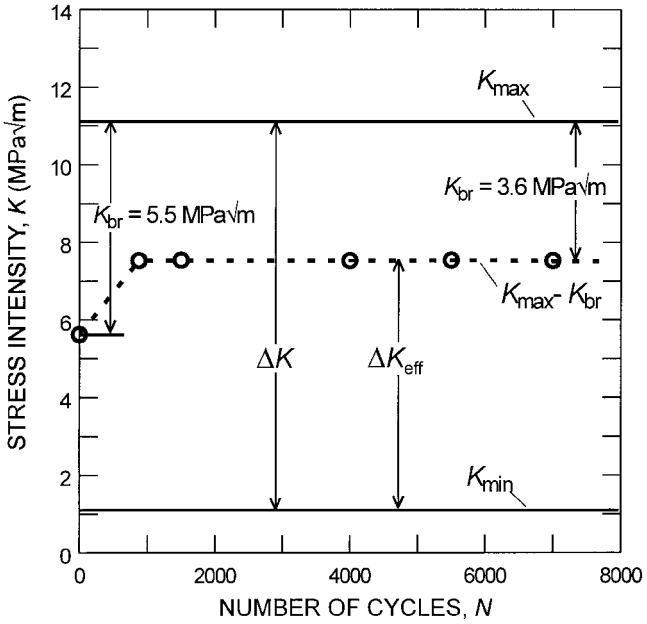

Fig. 10—The degradation, under cyclic loading, of a monotonically developed bridging zone in the MD fully lamellar microstructure is plotted in terms of K_{max}, K_{min}, and K_{max}-K_{br} as a function of the number of loading cycles, N. K_{br} = 5.5 MPa√m at that start of cyclic loading. After 875 loading cycles, this shielding term had decreased by 35 pct to K_{br} = 3.6 MPa√m. The degree of shielding provided by this bridging zone showed no further degradation out to 315,000 loading cycles.

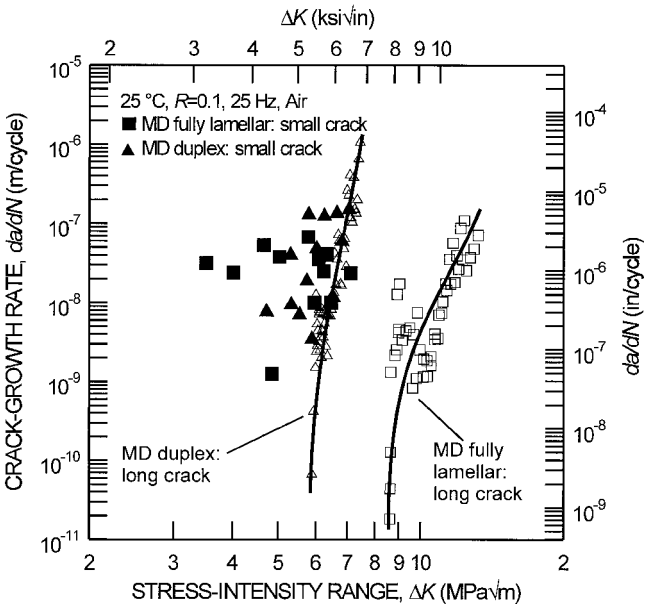

Fig. 11—Fatigue crack growth rates for through-thickness long cracks (a > 5 mm) and small surface cracks (c ~35 to 275 μm) in the MD fully lamellar and MD duplex microstructures. Small-crack data points represent average growth rate/ΔK combinations over a specific increment of crack extension (between two surface replications).

that afforded by ductile-phase ligaments, where extensive degradation and premature bridge failure can occur during fatigue crack growth.[32,46,47] It should be noted, however, that it is not known whether the mechanisms of formation of the uncracked ligaments are the same under monotonic and cyclic loading; consequently, the susceptibility of ligaments formed *during fatigue loading* to such degradation cannot be conclusively discussed.

3. *Small fatigue cracks*

Given the salient role of extrinsic crack-tip shielding mechanisms in the fatigue crack growth resistance of long cracks (>5 mm) in γ-TiAl–based alloys, particularly in the MD fully lamellar microstructure, it is likely that when crack sizes become comparable to the dimensions of the shielding zones, they will be susceptible to a similitude limitation.[53] In other words, by virtue of their limited wake, small cracks will not develop equilibrium shielding zones akin to long cracks. Consequently, at equivalent applied ΔK levels, the *local* driving force for crack growth, ΔK_{eff}, may be significantly higher for smaller crack sizes, such that small-crack growth rates may exceed the corresponding rates of long cracks and may propagate at applied ΔK levels below the long-crack threshold. Such behavior has been widely reported for metallic[54,55] and, more recently, for ceramic[56,57,58] materials. Since many potential applications of γ-TiAl–based alloys, *e.g.*, compressor blades, may be limited by such small-crack fatigue properties, the evaluation of this effect is of importance.

Fatigue crack growth rates for small semielliptical surface cracks (half-surface crack length of $c \sim 35$ to 275 μm) in the MD duplex and MD fully lamellar microstructures are plotted in Figure 11 as a function of the applied stress–intensity range; results for through-thickness long cracks (>5 mm) in compact-tension samples are presented for comparison. A number of points are worthy of note.

(1) Small-crack growth is observed in both structures at applied ΔK levels well below the long-crack threshold. Specifically, small-crack growth is evident at applied ΔK levels as low as 3.5 MPa√m in the MD fully lamellar structure, where the large-crack threshold is 8.6 MPa√m. Chan and Shih[48] have reported a similar small-crack effect in this same material, with small-crack growth occurring at ΔK levels as low as ~ 1 MPa√m. In the MD duplex structure, small cracks grow at applied ΔK levels as low as 4.7 MPa√m, compared to a long-crack threshold of 5.7 MPa√m.

(2) At equivalent applied ΔK levels, small-crack growth rates exceed those of corresponding long cracks by up to three orders of magnitude. Differences between long- and small-crack behavior, however, are greatly reduced in the duplex microstructure.

(3) The small-crack growth rates have characteristically far greater scatter than the corresponding long-crack results. This may be partly associated with experimental error; however, since the scatter is far more prominent in the coarser lamellar structure, it can be primarily associated with a biased sampling of the microstructure by flaws which are comparable in size to microstructural dimensions.[59]

(4) In marked contrast to long-crack behavior, where the MD fully lamellar structure has crack-growth resistance far superior to the duplex structure, the scatter bands of the small-crack data essentially overlap for the two microstructures. Indeed, the MD duplex structure may be considered to exhibit better small-crack properties, as the data are subject to less scatter and the minimum

applied ΔK levels at which small-crack growth is observed are higher than in the lamellar structure.

To verify quantitatively the significance of the similitude limitation, the experimentally measured shielding contributions from both uncracked ligament bridging and crack closure, in the form of K_{br} and K_{cl} values (Figure 7(a)), were ''subtracted'' from the long-crack data using Eq. [2]. As illustrated in Figure 12, replotting the long-crack data in terms of the closure- and bridging-corrected ΔK_{eff} results in a far closer correspondence between the long- and small-crack behavior.

The scaling of long- and small-crack data using ΔK_{eff} is less effective for the MD fully lamellar microstructure (Figure 12(a)), where several small-crack data points exist well below the long-crack effective threshold of $\Delta K_{TH,\text{eff}} = 5.5$ MPa$\sqrt{\text{m}}$. As noted previously, this behavior can be attributed to the comparable dimensions of the cracks and the lamellar colonies. For the small crack sizes in question, the crack front of an elliptical flaw would, at most, sample only a few lamellar colonies. Moreover, it is well documented that fatigue crack growth is influenced by lamellar orientation, with growth rates being faster, particularly at low ΔK levels, when crack advance is coplanar with the lamellar (γ/α_2) interface.[12,50,60,61] Thus, it is unlikely that a continuum parameter such as the long-crack threshold, which is determined for a through-thickness crack which samples many lamellar colonies, would reflect the worst-case growth-rate behavior of a small crack confined to only one or two colonies. In contrast, for the finer-scaled MD duplex microstructure, no small-crack growth was observed below the shielding-corrected long-crack threshold, $\Delta K_{TH,\text{eff}} = 4.3$ MPa$\sqrt{\text{m}}$ (Figure 12(b)).

Comparisons between the various lamellar and duplex microstructures investigated in this article clearly indicate the superior fracture toughness and cyclic crack-growth resistance for the lamellar microstructures. However, since the microstructural origins of this behavior result primarily from crack-tip shielding mechanisms, the superiority of the lamellar structures will only be observed when properties are evaluated with large cracks. Investigation of fatigue crack growth resistance in the presence of small cracks suggests the somewhat surprising result that, for most fatigue-critical applications for which γ-TiAl–based alloys are candidate materials, the duplex microstructure may, in fact, offer better properties. This microstructure is more amenable to reliable application in damage-tolerant design, has a higher fatigue limit,[3] and has better small-crack properties. Due to the very steep slope (high m) of the (long-crack) da/dN *vs* ΔK relationships for all these intermetallic alloys (Table IV), design will invariably have to be based on the concept of a threshold; thus, the ability to define a lower-bound fatigue threshold in the presence of small cracks (where shielding is ineffective) may well be a critical design parameter. The definition of such limits appears feasible for duplex microstructures in terms of a shielding-corrected long-crack threshold, at least for crack sizes larger than the characteristic microstructural dimensions (~20 μm). In fact, it has been shown in the MD duplex microstructure that this shielding-corrected threshold holds for small-crack sizes down to $c \sim 25$ μm.[62] In contrast, for the lamellar microstructures, there appears to be no benefit

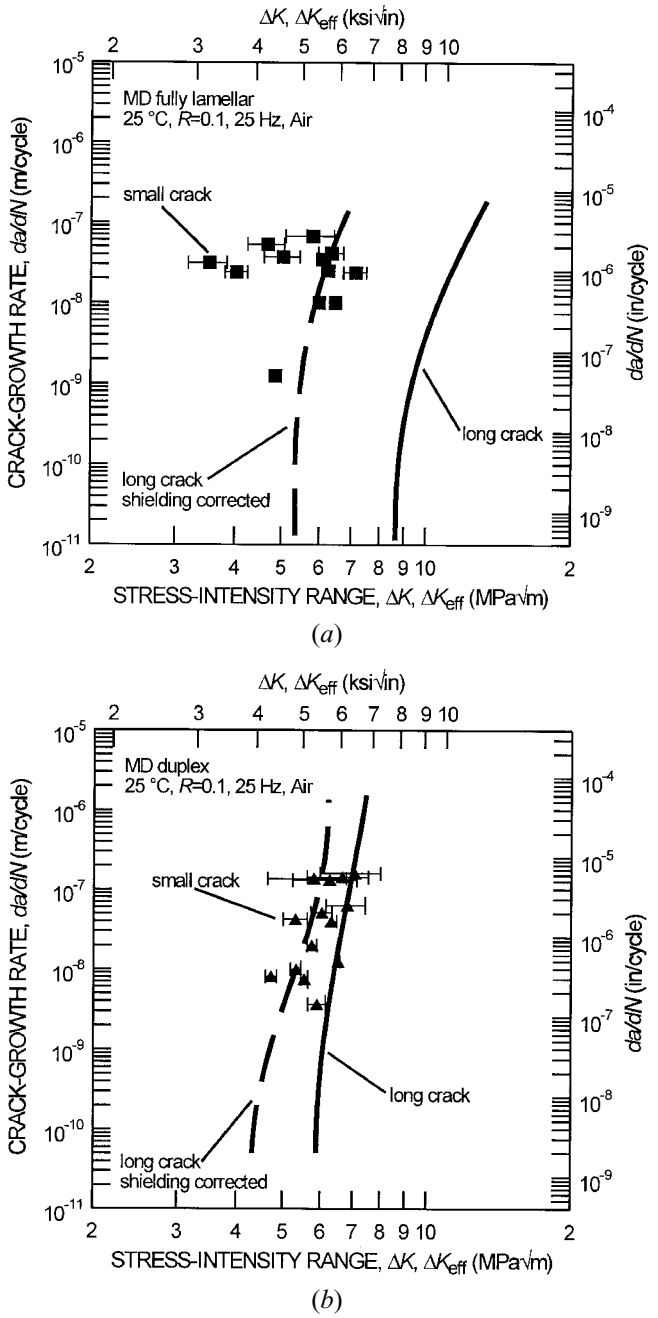

Fig. 12—Comparison of long-crack, small-crack, and shielding corrected long-crack fatigue data in the (*a*) MD fully lamellar and (*b*) MD duplex microstructures. Growth rates, da/dN, for the shielding corrected data are plotted as a function of ΔK_{eff} after accounting for the effect of both crack bridging and closure (refer to text). Error bars on the small-crack data represent the range of ΔK over the increment of measured crack growth.

over the duplex microstructure in terms of improved fatigue crack growth resistance *for small cracks*. Moreover, the definition of a lower-bound crack-growth threshold is considerably more difficult, as the characteristic microstructural dimensions are one order of magnitude larger. Accordingly, in these structures, the growth rates of small fatigue cracks up to ~300 μm in length are subject to considerable scatter, due to statistical sampling of the microstructure, and continue to propagate at stress intensity ranges well below the lower-bound (long-crack) $\Delta K_{TH,\text{eff}}$ threshold (Figure 12(a)).

IV. CONCLUSIONS

Based on a study of room-temperature fracture toughness and fatigue crack growth behavior in a range of γ-TiAl–based intermetallic alloys and microstructures, including duplex structures, fully lamellar structures with coarse and refined colony sizes, a lamellar structure with a refined colony size and lamellar spacing, a nearly lamellar structure with ~30 pct equiaxed γ phase and a refined colony size, and a single-phase γ microstructure, the following conclusions can be made.

1. Fracture toughness and (long-crack) fatigue crack growth resistance depend strongly on microstructure. In general, lamellar microstructures exhibit high toughnesses with significant R-curve behavior. Duplex microstructures have a lower toughness and negligible R-curve behavior. Lamellar microstructures also exhibit higher fatigue crack growth thresholds and superior *da*/*dN vs* ΔK behavior in the midgrowth-rate regime, provided the long-crack ($a > 5$ mm) data are characterized in terms of the applied stress intensity range.
2. The rank order of the various single-phase γ, duplex, and lamellar microstructures, in terms of crack-growth resistance, are found to be identical for fracture toughness and (long-crack) fatigue crack propagation behavior.
3. The superior R-curve behavior of the lamellar microstructures, as compared to the duplex microstructures, is attributed to the presence of uncracked ligament bridging in the crack wake, which acts to shield the crack tip from the far-field loading.
4. Significant toughness can be retained in a lamellar microstructure with refined colony size. The bridging zone in this refined lamellar microstructure is characterized by a larger number of smaller uncracked ligaments, as compared to a high-toughness, coarse lamellar structure (where the ligaments tend to be larger in size but fewer).
5. A deleterious effect of the equiaxed morphology of the γ phase on both fracture behavior and (long crack) fatigue crack growth resistance is observed. It is believed that the equiaxed γ phase degrades crack-growth resistance by inhibiting the action of uncracked ligament bridging and crack closure (in the case of fatigue).
6. Uncracked ligament bridges are found to form during fatigue crack growth in lamellar microstructures. Although the shielding contribution associated with these ligaments is significantly lower under cyclic fatigue loading compared to that observed under monotonic loading, significant shielding can be retained; *e.g.*, in the MD fully lamellar microstructure, K_{br} values as high as 14 pct of K_{max} were observed.
7. Based on studies in the MD alloy, differences in the fatigue crack growth resistance of the fully lamellar and duplex microstructures can be primarily attributed to enhanced crack-tip shielding (from crack closure and bridging) in the lamellar structure. Variations in the degree of shielding provided by these mechanisms are also largely responsible for the differences in fatigue crack growth resistance between the various lamellar microstructures investigated.
8. Growth rates for small surface cracks ($c \sim 35$ to 275 μm) in the MD fully lamellar and MD duplex microstructures are seen to exceed those of long ($a > 5$ mm) through-thickness cracks at the same applied ΔK levels; moreover, small cracks are found to propagate at stress intensity ranges below the nominal long-crack fatigue threshold.
9. This ''anomalous'' behavior of small cracks is attributed primarily to a limited role of crack-tip shielding, specifically from closure and uncracked ligament bridging, in cracks with limited wake. Accordingly, a closer correspondence between long- and small-crack data can be achieved by characterizing the long-crack data in terms of ΔK_{eff}, after ''correcting'' for the effect of crack closure and bridging.
10. A comparison of long-crack growth rates (as a function of ΔK) clearly demonstrates that the fatigue crack growth resistance of the fully lamellar microstructures is significantly greater than that of the duplex structures; in contrast, a comparison of small-crack data in the MD alloy indicates marginally superior fatigue crack growth resistance in the duplex structure (although the scatter bands for the two microstructures overlap). Additionally, the definition of a shielding-corrected (lower-bound) fatigue threshold, $\Delta K_{TH,eff}$, below which both long and small cracks will not propagate has been demonstrated in the duplex material; the ability to define such a threshold in the lamellar microstructure is complicated by the similarity in crack size and microstructural dimensions.

ACKNOWLEDGMENTS

This work was supported by the Air Force Office of Scientific Research under Grant Nos. F49620-93-1-0107 and F49620-96-1-0233, with Major C.H. Ward as contract monitor. Thanks are due to Major Ward for his support; J.J. Kruzic and S. Lillibridge for their assistance in obtaining the small-crack data; Drs. Y.-W. Kim (UES, Inc.), C.T. Liu (Oak Ridge National Laboratory), D.H. Shih (McDonnell-Douglas), and S.E. Hartfield-Wünsch (General Motors Corporation), for supplying the TiAl alloys; and the Office of Naval Research for a NDSEG Fellowship in support of JPC.

REFERENCES

1. Y.W. Kim: *JOM*, 1994, vol. 46 (7), pp. 30-40.
2. Y.-W. Kim and D.M. Dimiduk: *JOM*, 1991, vol. 43 (8), p. 40.
3. J.M. Larsen, B.D. Worth, S.J. Balsone, and J.W. Jones: in *Gamma Titanium Aluminides*, Y.-W. Kim, R. Wagner, and M Yamaguchi, eds., TMS, Warrendale, PA, 1995, pp. 821-34.
4. G.F. Harrison and M.R. Winstone: in *Mechanical Behavior of Materials at High Temperature*, C. Moura Branco, R.O. Ritchie, and V. Sklenicka, eds., Kluwer Academic Publishers, NATO ASI Series, 1996, pp. 309-25.
5. H.E. Dève, A.G. Evans, and D.S. Shih: *Acta Metall. Mater.*, 1992, vol. 40, pp. 1259-65.
6. K.T. Venkateswara Rao, Y.-W. Kim, C.L. Muhlstein, and R.O. Ritchie: *Mater. Sci. Eng.*, 1995, vol. A192, pp. 474-82.
7. S.J. Balsone, J.M. Larsen, D.C. Maxwell, and J.W. Jones: *Mater. Sci. Eng.*, 1995, vols. A192–A193, pp. 457-64.
8. K.S. Chan and Y.-W. Kim: *Metall. Trans. A*, 1992, vol. 23A, pp. 1663-77.
9. K.S. Chan: *Metall. Trans. A*, 1993, vol. 24A, pp. 569-83.

10. K.S. Chan and Y.-W. Kim: *Metall. Trans. A*, 1993, vol. 24A, pp. 113-25.
11. K.T. Venkateswara Rao, Y.-W. Kim, and R.O. Ritchie: *Scripta Metall. Mater.*, 1995, vol. 33, pp. 459-65.
12. D.L. Davidson and J.B. Campbell: *Metall. Trans. A*, 1993, vol. 24A, pp. 1555-74.
13. R. Gnanamoorthy, Y. Mutoh, K. Hayashi, and Y. Mizuhara: *Scripta Metall. Mater.*, 1995, vol. 33 (6), pp. 907-12.
14. C.T. Liu, P.J. Maziasz, D.R. Clemens, J.H. Schneibel, V.K. Sikka, T.G. Nieh, J. Wright, and L.R. Walker: in *Gamma Titanium Aluminides*, Y.-W. Kim, R. Wagner, and M. Yamaguchi, eds., TMS, Warrendale, PA, 1995, pp. 679-88.
15. K. Maruyama, R. Yamamoto, H. Nakakuchi, and N. Fujitsuna: *Mater. Sci. Eng.*, 1997, vols. A239–A240, pp. 419-28.
16. Y.Q. Sun: *Mater. Sci. Eng.*, 1997, vols. A239–A240, pp. 131-36.
17. H. Umeda, K. Kishida, H. Inui, and M. Yamaguchi: *Mater. Sci. Eng.*, 1997, vols. A239–A240, pp. 336-43.
18. J.P. Campbell, A.L. McKelvey, S. Lillibridge, K.T. Venkateswara Rao, and R.O. Ritchie: in *Deformation and Fracture of Ordered Intermetallic Materials III*, W.O. Soboyejo, T.S. Srivatsan, and H.L. Fraser, eds., TMS, Warrendale, PA, 1996, pp. 141-57.
19. G. Malakondaiah and T. Nicholas: *Metall. Mater. Trans. A*, 1996, vol. 27A, pp. 2239-51.
20. H. Baiyun, H. Yuehui, Z. Kechao, Q. Xuanhui, and C. Xiaoqun: *Mater. Sci. Eng.*, 1997, vols. A239–A240, pp. 709-12.
21. K. Ichikawa and Y. Kinoshita: *Mater. Sci. Eng.*, 1997, vols. A239–A240, pp. 493-502.
22. T.K. Lee, E.I. Mosunov, and S.K. Hwang: *Mater. Sci. Eng.*, 1997, vols. A239–A240, pp. 540-45.
23. K.S. Kumar, J.A.S. Green, J.D.E Larsen, and L.D. Kramer: *Adv. Mater. Proc.*, 1995, vol. 148 (4), pp. 35-38.
24. D.E. Larsen: in *Microstructure/Property Relationships in Titanium Aluminides and Alloys*, Y.-W. Kim and R.R. Boyer, eds., TMS, Warrendale, PA, 1991, pp. 345-53.
25. W. Elber: *Eng. Fract. Mech.*, 1970, vol. 2, pp. 37-45.
26. R.O. Ritchie and W. Yu: in *Small Fatigue Cracks*, R.O. Ritchie and J. Lankford, eds., TMS-AIME, Warrendale, PA, 1986, pp. 167-89.
27. R.O. Ritchie, W. Yu, and R.J. Bucci: *Eng. Fract. Mech.*, 1989, vol. 32, pp. 361-77.
28. W.F. Deans and C.E. Richards: *J. Test. Eval.*, 1979, vol. 7, pp. 147-54.
29. C.E. Richards and W.F. Deans: in *The Measurement of Crack Length and Shape during Fracture and Fatigue*, C.J. Beevers, ed., EMAS Ltd., Warley, United Kingdom, 1980, pp. 28-68.
30. D.C. Maxwell: Materials Laboratory, Air Force Wright Aeronautical Laboratories, Report No. AFWAL-TR-87-4046, Wright-Patterson Air Force Base, Dayton, OH, 1987.
31. J.C. Newman and I.S. Raju: *Eng. Fract. Mech.*, 1981, vol. 15, pp. 185-92.
32. K.T. Venkateswara Rao, G.R. Odette, and R.O. Ritchie: *Acta Metall. Mater.*, 1994, vol. 42, pp. 893-911.
33. K.S. Chan: *Metall. Trans. A*, 1991, vol. 22A, pp. 2021-29.
34. K.S. Chan: *Metall. Trans. A*, 1995, vol. 26A, pp. 1407-18.
35. K.S. Chan: *JOM*, 1992, vol. 44 (5), pp. 30-48.
36. K.S. Chan and Y.-W. Kim: *Metall. Mater. Trans. A*, 1994, vol. 25A, pp. 1217-28.
37. H.E. Dève and A.G. Evans: *Acta Metall. Mater.*, 1991, vol. 39 (6), pp. 1171-76.
38. N.J. Rogers and P. Bowen: in *Structural Intermetallics*, R. Darolia, J.J. Lewandowski, C.T. Liu, P.L. Martin, D.B. Miracle, and M.V. Nathal, eds., TMS, Warrendale, PA, 1993, pp. 231-40.
39. C.T. Liu, J.H. Schneibel, P.J. Maziasz, J.L. Wright, and D.S. Easton: *Intermetallics*, 1996, vol. 4, pp. 429-40.
40. M.G. Jenkins, A.S. Kobayashi, K.W. White, and R.C. Bradt: *Int. J. Fract.*, 1987, vol. 34, pp. 281-95.
41. K.S. Chan and Y.-W. Kim: *Acta Metall. Mater.*, 1995, vol. 43, pp. 439-51.
42. K.S. Chan: in *Gamma Titanium Aluminides*, Y.-W. Kim, R. Wagner, and M. Yamaguchi, eds., TMS, Warrendale, PA, 1995, pp. 875-82.
43. S.L. Kampe, P. Sadler, D.E. Larsen, and L. Christodoulou: in *Microstructure/Property Relationships in Titanium Aluminides and Alloys*, Y.-W. Kim and R. Boyer, eds., TMS, Warrendale, PA, 1991, pp. 313-22.
44. A.G. Evans: *J. Am. Ceram. Soc.*, 1990, vol. 73, pp. 187-206.
45. R.O. Ritchie: *Mater. Sci. Eng.*, 1988, vol. A103, pp. 15-28.
46. K. Badrinarayanan, A.L. McKelvey, K.T. Venkateswara Rao, and R.O. Ritchie: *Metall. Mater. Trans. A*, 1996, vol. 27A, pp. 3781-92.
47. D.R. Bloyer, K.T. Venkateswara Rao, and R.O. Ritchie: in *Layered Materials for Structural Applications*, J.J. Lewandowski, C.H. Ward, M.R. Jackson, and J.W.H. Hunt, eds., MRS, Pittsburgh, PA, 1996, pp. 243-48.
48. K.S. Chan and D.S. Shih: *Metall. Mater. Trans. A*, 1997, vol. 28A, pp. 79-90.
49. K.S. Chan and D.S. Shih: *Metall. Mater. Trans. A*, 1998, vol. 29A, pp. 73-87.
50. D.J. Wissuchek, G.E. Lucas, and A.G. Evans: in *Gamma Titanium Aluminides*, Y.-W. Kim, R. Wagner, and M. Yamaguchi, eds., TMS, Warrendale PA, 1995, pp. 875-82.
51. S. Suresh: *Metall. Trans. A*, 1985, vol. 16A, pp. 249-60.
52. C.J. Gilbert, R.H. Dauskardt, and R.O. Ritchie: *J. Am. Ceram. Soc.*, 1995, vol. 78, pp. 2291-2300.
53. J.P. Campbell, J.J. Kruzic, S. Lillibridge, K.T. Venkateswara Rao, and R.O. Ritchie: *Scripta Mater.*, 1997, vol. 37, p. 707.
54. S. Suresh and R.O. Ritchie: *Int. Met. Rev.*, 1984, vol. 29, pp. 445-76.
55. R.O. Ritchie and J. Lankford: *Mater. Sci. Eng.*, 1986, vol. A84, pp. 11-16.
56. R.H. Dauskardt, M.R. James, J.R. Porter, and R.O. Ritchie: *J. Am. Ceram. Soc.*, 1992, vol. 75, pp. 759-71.
57. R.H. Dauskardt, R.O. Ritchie, J.K. Takemoto, and A.M. Brendzel: *J. Biomedical Mater. Res.*, 1994, vol. 28, pp. 791-804.
58. A.A. Steffen, R.H. Dauskardt, and R.O. Ritchie: *J. Am. Ceram. Soc.*, 1991, vol. 74, pp. 1259-68.
59. K.T. Venkateswara Rao, W. Yu, and R.O. Ritchie: *Eng. Fract. Mech.*, 1988, vol. 31, pp. 623-35.
60. P. Bowen, R.A. Chave, and A.W. James: *Mater. Sci. Eng.*, 1995, vols. A192–A193, pp. 443-56.
61. P. Bowen, N.J. Rogers, and A.W. James: in *Gamma Titanium Aluminides*, Y.-W. Kim, R. Wagner, and M. Yamaguchi, eds., TMS, Warrendale, PA, 1995, pp. 849-65.
62. J.J. Kruzic: Master's. Thesis, University of California at Berkeley, Berkeley, CA, May 1998.